Original Research

Image Construction Methods for Phased Array Magnetic Resonance Imaging

Deniz Erdogmus, PhD,[1]* Rui Yan,[1] Erik G. Larsson, PhD,[2] Jose C. Principe, PhD,[1] and Jeffrey R. Fitzsimmons, PhD[3]

Purpose: To study image construction in phased array magnetic resonance imaging (MRI) systems from a statistical signal processing point of view.

Materials and Methods: Three new approaches for image combination with multiple coils are proposed: 1) one based on the singular value decomposition of the measurement matrix, which is asymptotically optimal in the signal-to-noise ratio sense; 2) one based on a maximum-likelihood formulation, incorporating a priori information on the coil sensitivities in a Bayesian manner; and 3) one based on a least-squares formulation, which incorporates a smoothness constraint on the coil sensitivities.

Results: Numerical examples using synthetic and real data are presented to illustrate the performance of these new approaches. Results on the synthetic data show improvement in signal-to-error ratio, while results on the real data (a 4.7 T four-coil image of a cat spinal cord) show that the proposed methods can improve the SNR in the final image by up to 3 dB in the regions of interest compared to conventional sum-of-squares processing.

Conclusion: It is demonstrated that phased array MRI reconstruction performance can be improved by the use of more elaborate statistical signal processing algorithms.

Key Words: statistical signal processing; Bayesian MR image reconstruction; phased-array MRI; singular value decomposition, MR image reconstruction; least-squares, MR image reconstruction
J. Magn. Reson. Imaging 2004;20:306–314.

MAGNETIC RESONANCE IMAGING (MRI) as a noninvasive diagnostic tool is one of the most significant breakthroughs experienced by the medical community during the past century. Conventionally, MRI has primarily been used for imaging of static scenarios, but recently it has also been used with great success for imaging time-varying processes. An important application of dynamic MRI is imaging of the heart and monitoring of cardiac diseases (1). Another example of dynamic imaging is functional MRI (fMRI), where the time-variability of certain chemical compositions—for example, in the brain—is investigated when the patient is subjected to an external stimulus. For these applications, the image acquisition speed is a critical limiting factor.

While MRI originally involved a strong magnet and a radio antenna (referred to as a coil), recent advances introduced multiple coils, called phased array coils. The phased array coils bring at least two benefits: first, by appropriately combining the signals from different coils, the signal-to-noise ratio (SNR) and the image quality can be improved; second, by using proper phased array imaging techniques, imaging times can be reduced significantly, therefore increasing cost-effectiveness, reducing motion artifacts, and decreasing the discomfort for patients. In addition, it is usually possible to trade image quality against acquisition speed. One of the first phased-array MRI systems was implemented and studied by Roemer et al (2), but the idea of using multiple coils can be traced further back (3). A complete treatment of the history of phased array imaging is outside the scope of this discussion, but representative examples of early work include can be found in the literature (4–8); a good summary of this literature is provided by Wright and Wald (9). More recently, a substantial body of research has focused on sophisticated techniques for phase encoding together with the use of gradient coils (with the primary aim of increasing the imaging speed). This work includes the sensitivity encoding for fast MRI (SENSE) technique (10) and its extensions (11), along with the related simultaneous acquisition of spatial harmonics (SMASH) method (12–15), as well as the partially parallel imaging with localized sensitivities (PILS) technique (16).

The literature on phased array MRI thus far does not approach the problem of image reconstruction using measurements from multiple coils from a statistical signal processing standpoint. The main objective of this study was to study the phased-array imaging problem in a statistical signal processing framework, and to

[1]Department of Electrical and Computer Engineering, University of Florida, Gainesville, Florida.
[2]Department of Electrical and Computer Engineering, The George Washington University, Washington, District of Columbia.
[3]Department of Radiology, University of Florida, Gainesville, Florida.
Contract grant sponsor: NSF; Contract grant number: ECS-0300340.
*Address reprint requests to: D.E., University of Florida, NEB 486, Gainesville, FL 32611. E-mail: deniz@cnel.ufl.edu
Received May 8, 2003; Accepted April 19, 2004.
DOI 10.1002/jmri.20115
Published online in Wiley InterScience (www.interscience.wiley.com).

discuss some difficulties associated with this approach. In conjunction with this goal, three image combination methods that are optimal in either the least-squares sense or the maximum-likelihood sense are presented. These proposed methods exploit the observed (or known) statistical and structural properties of the spatial coil sensitivity profiles. Our goal is to identify alternative image reconstruction algorithms that can improve SNR in the reconstructed images; thus, this paper does not deal with the imaging speed issues.

MATERIALS AND METHODS

Phased Array Signal Model

The physics underlying MRI is described by a vector differential equation called the Bloch equation (17). After appropriate sampling and transformation procedures, it can be shown that, for the k^{th} coil, the complex-valued received signal $s_k(i,j)$ at spatial coordinates (i,j) is given by (18–20):

$$s_k(i,j) = \rho(i,j)c_k(i,j) + n_k(i,j) \tag{1}$$

where $\rho(i,j)$ is the desired image intensity, $c_k(i,j)$ is the complex-valued coil sensitivity, and $n_k(i,j)$ is complex-valued (Gaussian), wide sense stationary (WSS), zero-mean, spatially white noise, which is possibly correlated across coils with covariance matrix $\mathbf{\Psi}$ (spatiotemporally constant due to the WSS assumption) (2,21,22). Note that the noise correlation, if properly compensated for, does not pose a limitation to the achievable image quality (23). In this signal model, the specific values of the coil sensitivities are, in general, not known. However, some a priori knowledge in the form of statistical distributions or structural constraints (such as spatial smoothness) may be available.

Known Coil Sensitivities

It is well-known in the statistical signal processing literature that for complex-valued received signals, assuming that the coil sensitivities are known, the SNR-optimal linear combination of the measurements for estimating $\rho(i,j)$ is given by:

$$\hat{\rho}(i,j) = \frac{\mathbf{c}^H(i,j)\mathbf{\Psi}^{-1}\mathbf{s}(i,j)}{\mathbf{c}^H(i,j)\mathbf{\Psi}^{-1}\mathbf{c}(i,j)} \tag{2}$$

where ^{H} denotes the conjugate-transpose (Hermitian) operation, $\mathbf{c}(i,j)$ is the vector of coil sensitivities, and $\mathbf{s}(i,j)$ is the vector of measurements for pixel (i,j). The SNR-optimality of this reconstruction method among all linear combiners can be proved, for example, by applying the Cauchy-Schwartz inequality (24), and the SNR for this reconstruction method can be determined to be $|\rho|^2\|\mathbf{c}\|^2/\sigma^2$, where σ^2 is the noise power (of both real and imaginary parts).

Unknown Coil Sensitivities

In practice, the coil sensitivities $\mathbf{c}(i,j)$ are unknown. Furthermore, they depend on the coupling between the receiver and the sample; therefore, they are often hard to determine accurately via electromagnetic theory or calibration, in particular for high field strengths.

In the case of unknown coil sensitivities, perhaps the most commonly used reconstruction technique is sum-of-squares (SoS). With this method, the data is first pre-whitened with $\mathbf{\Psi}^{-1/2}$ to eliminate the noise covariance. For SoS, the reconstructed pixel value is therefore given by:

$$\hat{\rho}(i,j) = (\mathbf{s}^H(i,j)\mathbf{s}(i,j))^{1/2} \tag{3}$$

Clearly, as the noise power approaches to zero, the SoS estimate approaches $\hat{\rho}(i,j) = |\rho(i,j)|(\mathbf{c}^H(i,j)\mathbf{c}(i,j))^{1/2}$, and hence it yields, in general, a biased estimate. Although this bias is clearly spatially varying, because the magnitude of the complex valued coil sensitivity is spatially varying, in general, the asymptotic SNR for SoS can be found to be identical to that of the optimal linear combiner (25), which is an appealing property.

A number of techniques for phased array image construction have appeared during the last decade. For example, as an alternative to SoS, Debbins et al (26) suggested adding the images coherently after their relative phases are properly adjusted. Bydder et al (27) proposed a method that attempts to estimate the coil sensitivities from the image; although the resulting image has somewhat less variance than SoS, it still suffers from bias. Kellman and McVeigh (28) proposed a method that can use the degrees of freedom inherent to the phased array for ghost artifact cancellation. Walsh et al (29) proposed an algorithm to improve SNR using an adaptive filtering framework. However, despite the innovative techniques presented in these papers, a fully optimal image recombination method for unknown coil sensitivities appears yet to be discovered.

Reconstruction Methods Using Prior Information on Coil Sensitivities

In this section, we present three image reconstruction methods for phased array MRI that are optimal in the least-squares or maximum-likelihood sense. To this end, one of the following two assumptions will be made:

A1. The coil sensitivities remain approximately constant over a small region Ω consisting of N pixels, i.e., $\mathbf{c}(i,j) = \mathbf{c}$ for $(i,j) \in \Omega$.
A2. The coil sensitivity profiles vary smoothly with the spatial location, within the regions of interest.

In order to justify these assumptions, consider the images of a cat spinal cord shown in Fig. 1a–d taken using the four-coil phased array shown in Fig. 1e (4.7 T, TR = 1000 msec, TE = 15 msec, field of view [FOV] = 10 × 5 cm, matrix = 256 × 128, slice thickness = 2 mm, sweep width = 26 kHz, one average). Regarding SoS as a linear combination methodology, the equivalent coil sensitivity estimates produced by this algorithm are found to be:

$$\hat{\mathbf{c}}(i,j) = \mathbf{s}(i,j)(\mathbf{s}^H(i,j)\mathbf{s}(i,j))^{-1/2} \tag{4}$$

These estimated coil sensitivity profiles generated by SoS are also shown in Fig. 1f–i, as well as the recon-

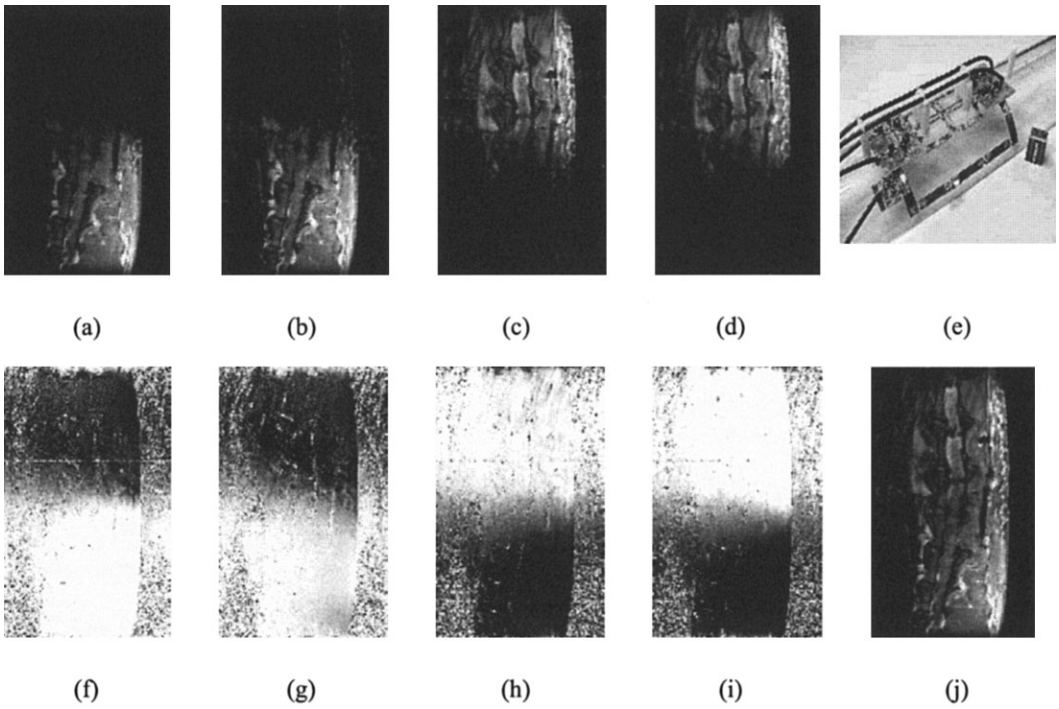

Figure 1. The image obtained from coil 1 (**a**), coil 2 (**b**), coil 3 (**c**), and coil 4 (**d**), where the measurements are obtained using the phased array shown in **e**. The coil sensitivity estimates for coil 1 (**f**), coil 2 (**g**), coil 3 (**h**), and coil 4 (**i**), and the reconstructed image obtained using the SoS reconstruction method (**j**).

structed image estimate (Fig. 1j). Notice in Fig. 1f–i that the four spatial coil sensitivity profiles exhibit a quite smooth behavior as a function of the spatial coordinates.

A similar structural behavior of the coil sensitivity profiles has also been observed in images of various other objects, including phantoms and human tissues. This observation is the main motivation behind the two assumptions stated above. The three reconstruction methods that are proposed below take advantage of this structural quality of the coil sensitivities over space to generate optimal results in a statistical array signal processing framework under the assumptions stated.

Singular Value Decomposition (SVD)

For a phased array imaging system consisting of n_c coils, under assumption A1 the data model for some small region Ω simplifies to the following vector-matrix equation:

$$\mathbf{S} = \rho\mathbf{c}^T + \mathbf{N} \tag{5}$$

where ρ is the vector of pixel values in the region, $\mathbf{S} = [\mathbf{s}_1 \ldots \mathbf{s}_{n_c}]$ is the measurement matrix of size $N \times n_c$, and $\mathbf{N}$ is the noise matrix (of the same size as $\mathbf{S}$) consisting of independent samples across pixels, but possibly correlated across coils.

In the ideal noise-free case, $\mathbf{S}$ has rank one, and the left and right singular vectors of $\mathbf{S}$ are ρ and $\mathbf{c}$, respectively. However, the presence of noise increases the rank of $\mathbf{S}$; hence, the left singular vector and the right singular vector corresponding to the maximum singular value will yield the least squares estimates of ρ and $\mathbf{c}$ (24). Specifically, if

$$\mathbf{S} = [\mathbf{u}_1 \ldots \mathbf{u}_{n_c}] \begin{bmatrix} \lambda_1 & 0 & 0 \\ 0 & \ddots & 0 \\ 0 & 0 & \lambda_{n_c} \end{bmatrix} \begin{bmatrix} \mathbf{v}_1^T \\ \vdots \\ \mathbf{v}_{n_c}^T \end{bmatrix} = \mathbf{U}\,\Sigma\,\mathbf{V}^T \tag{6}$$

is the SVD of $\mathbf{S}$, then $\mathbf{u}_1$ and $\mathbf{v}_1$ minimize $\|\mathbf{S} - \mathbf{u}_1\lambda_1\mathbf{v}_1^T\|^2$ (in Eq. [6], $\mathbf{U}$ and $\mathbf{V}$ are orthonormal singular vector matrices and Σ is a diagonal matrix that contains the singular values in descending order). The unit-power estimate of the image in region Ω is therefore $\hat{\rho} = \mathbf{u}_1$ and the corresponding coil sensitivity vector estimate for this region is $\hat{\mathbf{c}} = \Sigma^{1/2}\mathbf{v}_1$. Obviously, the scale factor contained in the first singular value could be distributed between ρ and $\mathbf{c}$ in infinitely many ways, resulting in a scale ambiguity for the image in this region. This problem could be solved, for example, by using the scale factor obtained via the SoS solution for this region, or by using techniques borrowed from Murakami et al (30). The procedure must be repeated for all regions in the whole image. Using eigenvalue perturbation theory, the asymptotic SNR of this method can be found to be identical to that of optimal linear combining. The second assumption used in this approach (besides A1) is A3: The measurement matrix has an effective rank of one. Effectively, this is equivalent to assuming that the coil measurement SNR levels are sufficiently high. In the noise-free measurement case, A1 implies A3.

In order to demonstrate the validity of this assumption, we resort to the same cat spinal cord image example shown in Fig. 1. Figure 2a shows the histogram of

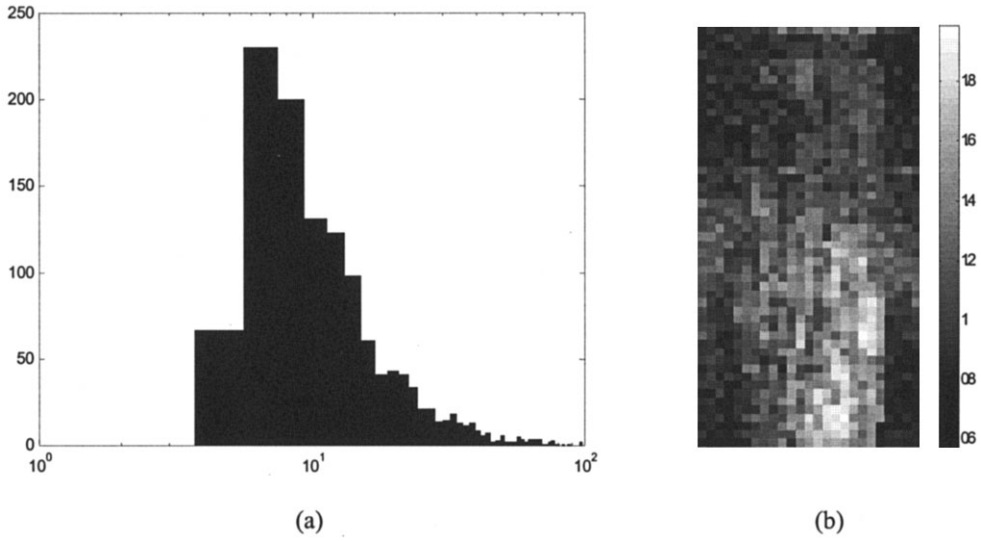

Figure 2. The ratio of the maximum singular value to the average of the smaller three singular values of the measurement matrices for 5×5 non-overlapping regions summarized in a histogram (**a**) and depicted as a spatial distribution over the image (**b**) with grayscale values assigned in $\log_{10}$ scale, with brighter values representing higher ratios.

the ratio between the largest singular value of the local measurement matrix to the mean of the other three singular values (there are four singular values because there are four coils). Because there are very few small singular value ratios, we conclude that in most local regions the rank-one measurement matrix assumption accurately holds. In fact, the noise-only regions dominantly contribute to the small singular-value-ratios. To illustrate this fact, in Fig. 2b we also present the singular-value-ratio as a function of spatial coordinate for the cat-spine image, using 5×5 square local regions.

Bayesian Maximum-Likelihood (ML) Reconstruction

The Bayesian ML reconstruction approach also relies on assumption A1; therefore, it operates on a set of small regions that constitute a partitioning for the whole image. In addition, any available statistical information about the coil sensitivities and noise in the form of probability distribution functions (pdf) are incorporated in the formulation. This is stated formally in the following assumption. A4: Sufficiently accurate a priori information regarding the probability distribution function of the coil sensitivities and the additive measurement noise is available.

The principle behind ML reconstruction is to maximize the a posteriori probability of the observed data given the image pixel values, and is formulated in the following optimization problem:

$$\hat{\rho} = \arg\max_{\rho} p(\mathbf{S}|\rho) = \int p(\mathbf{S},\mathbf{c}|\rho)d\mathbf{c} = \int p(\mathbf{S}|\mathbf{c},\rho)p(\mathbf{c})d\mathbf{c} \quad (7)$$

Here, $p(\mathbf{S}|\rho)$ is the conditional pdf of the measurement matrix given the image, $p(\mathbf{S},\mathbf{c}|\rho)$ is the joint pdf of the measurement matrix and the coil sensitivity vector conditioned on the image, $p(\mathbf{S}|\mathbf{c},\rho)$ is the conditional pdf of the measurement matrix given the coil sensitivity vector and the image, and finally, $p(\mathbf{c})$ is the pdf of the coil sensitivity vector.[1] Assuming that the noise in the measurements is jointly Gaussian, we have:

$$p(\mathbf{S}|\mathbf{c},\rho) = \pi^{-Nn_c}|\mathbf{Q}|^{-n_c} \exp(-\|(\mathbf{S} - \rho\mathbf{c}^T)\mathbf{Q}^{-1/2}\|^2) \quad (8)$$

A Gaussian noise distribution can often be justified by invoking the central limit theorem (31). In addition, ML formulations with Gaussian disturbance terms tend to give rise to mathematically convenient expressions, often in a least-squares form, which are often intuitively appealing. (For instance, it is not hard to show that the max-SNR reconstruction of Eq. [2] is equivalent to ML if the noise is Gaussian.) If we further assume that the density of $\mathbf{c}$ is also Gaussian with mean μ and covariance Λ, the conditional pdf of the observed data becomes:[2]

$$p(\mathbf{S}|\rho) = (\pi^{-(N+1)n_c}|\mathbf{Q}|^{-n_c}|\Lambda|^{-1}) \int \exp(-\|(\mathbf{S} - \rho\mathbf{c}^T)\mathbf{Q}^{-1/2}\|^2 - \|\Lambda^{-1/2}(\mathbf{c} - \mu)\|^2) \quad (9)$$

The incorporation of a priori knowledge about model parameters via Bayesian statistics has the advantage that the uncertainty in the value can be controlled by adjusting the covariance matrix Λ. For example, a situation with little initial knowledge about the value of $\mathbf{c}$ can be represented by a matrix Λ with large eigenvalues. On the other hand, setting $\Lambda = \mathbf{0}$ results in a least-square optimal estimation of ρ corresponding to $\mathbf{c} = \mu$. A fixed-point algorithm for maximizing the quantity in Eq. [9] is described in Appendix A.

[1]Note that if a priori information about ρ is available (which is however unlikely) in the form of a pdf, $p(\rho)$, it can be incorporated in the optimization problem in EQ. [7] by multiplying it with $p(\mathbf{S}|\rho)$ to result in a reconstruction that is optimal in the maximum a posteriori (MAP) sense.

[2]The randomness assumption for $\mathbf{c}$ emanates from the fact that it is a spatially varying unknown parameter. In Bayesian estimation theory, unknown deterministic parameters are typically treated as random variables.

In an MRI application, we may obtain ρ and $\mathbf{c}$ either via analytical modeling of the electromagnetic fields associated with the coils, or via calibration scans of a phantom with known contrasts; by modulating the parameter Λ, we can directly influence the accuracy of the prior knowledge of $\mathbf{c}$. Such efforts to compute the coil sensitivity patterns must use the "finite-difference time-domain" (FDTD) method, which is a computational method to solve Maxwell's equations. FDTD divides the problem space into rectangular cells, called Yee-cells, and uses discrete time-steps (32,33). This approach has been successfully employed to compute the sensitivity patterns of transmit and receive coils for MRI (34). The noise covariance, on the other hand, can be estimated from the coil images using portions of the frame that do not have any signal.

Because a closed-form expression for the solution of this reconstruction algorithm is not available, it is difficult to obtain an asymptotic SNR expression. Nevertheless, because the solution is the fixed-point of the iterations given in Appendix A, perturbation methods could be used to obtain an SNR expression, possibly after tedious calculations:

$$\begin{aligned}
\mathcal{J}(\rho,\mathbf{c}_1,\ldots,\mathbf{c}_{n_c}) &= (1-\lambda_1-\lambda_2-\lambda_3)\mathcal{J}_0(\rho,\mathbf{c}_1,\ldots,\mathbf{c}_{n_c}) \\
&\quad + \lambda_1\mathcal{J}_1(\mathbf{c}_1,\ldots,\mathbf{c}_{n_c}) + \lambda_2\mathcal{J}_2(\mathbf{c}_1,\ldots,\mathbf{c}_{n_c}) + \lambda_3\mathcal{J}_3(\rho) \\
\mathcal{J}_0(\rho,\mathbf{c}_1,\ldots,\mathbf{c}_{n_c}) &= \sum_{k=1}^{n_c}\sum_{i=1}^{M_1}\sum_{j=1}^{M_2}[\mathbf{s}_k(i,j)-\rho(i,j)\mathbf{c}_k(i,j)]^2 \\
&= \sum_{k=1}^{n_c}\|\mathbf{s}_k-\rho\circ\mathbf{c}_k\|^2 \\
\mathcal{J}_1(\mathbf{c}_1,\ldots,\mathbf{c}_{n_c}) &= \sum_{k=1}^{n_c}\sum_{i=2}^{M_1}\sum_{j=1}^{M_2}[\mathbf{c}_k(i,j)-\mathbf{c}_k(i-1,j)]^2 \\
&\quad + \sum_{k=1}^{n_c}\sum_{i=1}^{M_1}\sum_{j=2}^{M_2}[\mathbf{c}_k(i,j)-\mathbf{c}_k(i,j-1)]^2 \\
&= \sum_{k=1}^{n_c}(\|\mathbf{A}_1\mathbf{c}_k\|^2+\|\mathbf{A}_2\mathbf{c}_k^T\|^2) \\
\mathcal{J}_2(\mathbf{c}_1,\ldots,\mathbf{c}_{n_c}) &= \sum_{k=1}^{n_c}\sum_{i=3}^{M_1}\sum_{j=1}^{M_2}\begin{bmatrix}\mathbf{c}_k(i,j)-2\mathbf{c}_k(i-1,j)\\ +\mathbf{c}_k(i-2,j)\end{bmatrix}^2 \\
&\quad + \sum_{k=1}^{n_c}\sum_{i=1}^{M_1}\sum_{j=3}^{M_2}\begin{bmatrix}\mathbf{c}_k(i,j)-2\mathbf{c}_k(i,j-1)\\ +\mathbf{c}_k(i,j-2)\end{bmatrix}^2 \\
&= \sum_{k=1}^{n_c}(\|\mathbf{B}_1\mathbf{c}_k\|^2+\|\mathbf{B}_2\mathbf{c}_k^T\|^2) \\
\mathcal{J}_3(\rho) &= \sum_{i=1}^{M_1}\sum_{j=1}^{M_2}[\rho(i,j)]^2 = \|\rho\|^2 \qquad (10)
\end{aligned}$$

Least Squares (LS) with Smoothness Penalty

Given the measurement model in Eq. [1] and assumption A2, a simple and intuitive approach is to solve a penalized LS problem to reconstruct the image from the coil measurements. Recall that LS methods coincide with ML if the error is Gaussian. A natural smoothness penalty function is one that attempts to minimize the first and second order spatial derivatives of the coil sensitivities. However, such an approach alone does not solve the problem, because the optimal solution of a penalized LS criterion tends to yield images with large intensity. This is so because decreasing the amplitude of the coil sensitivity profile decreases its derivatives as well, causing the reconstructed image to be scaled up by the same amount. Therefore, it appears necessary to also impose a penalty on the total energy of the image. The resulting penalized least squares criterion, which has to be minimized to obtain the optimal reconstructed image, is given in Eq. [10], where ρ now denotes the vector of pixel values for the whole image; hence, no partitioning is required here. Note that the penalty term in this LS formulation can be interpreted as a Bayesian prior on the smoothness in conjunction with the form in Eq. [A.1]) (35).[3] In general, LS criteria can be shown to be equivalent to the maximum likelihood principle if the probability distributions under consideration are Gaussian, or perhaps other symmetric unimodal functions where the peak of the distribution corresponds to its mean value as well (36).

RESULTS

The performances of the proposed algorithms were first evaluated using synthetic data. The data model for this data is as follows. A random image consisting of nine pixels whose j^{th} pixel value is drawn from Uniform $[j, j+1]$ and then normalized such that the norm of the intensity vector is unity, $\rho^T\rho = 1$. The measurement vector in each coil is obtained by $\mathbf{s}_k = (\rho + \sigma\cdot\mathbf{e}_k)c_k$, where $\mathbf{c} = [c_1,\ldots,c_4]^T$ is the coil sensitivity vector (with each entry selected from Uniform [0,1]), $\mathbf{e}_k$ is zero-mean, unit-covariance Gaussian noise (also independent across coils), and σ is the SD of the additive noise determined by the specific measurement SNR that is being simulated.[4] All four algorithms (SVD, ML, LS, and SoS) are applied to this synthetic data in 20,000 Monte-Carlo simulations for each measurement SNR level, where all parameters are randomized as described above in every trial.

The image intensity estimate vectors of all four algorithms are normalized to unity such that in the comparison with the "ground truth" (which is available in this setup) using signal-to-error ratio (SER) scaling errors are not a factor. The SER is defined as SER (dB) = $101\log_{10}(\|\rho\|^2/\|\rho-\hat{\rho}\|^2)$, where $\hat{\rho}$ is the normalized estimate obtained using the corresponding algorithm. The results of this Monte-Carlo experiment on the described

[3]More details on the relation between smoothness constraints and a priori information via Bayesian statistics can be found in the literature (34).

[4]Note that this is not a very realistic situation, because in actual MRI the measurement SNR in a coil is also determined by its sensitivity coefficient. In this example, however, the noise is added to the image before coil sensitivity scaling is applied merely for convenience in representing results (such that a single SNR value describes the data quality). In fact, it will become evident in the application to real data that statistical signal processing approaches benefit more from this variability in measurement SNR of coils.

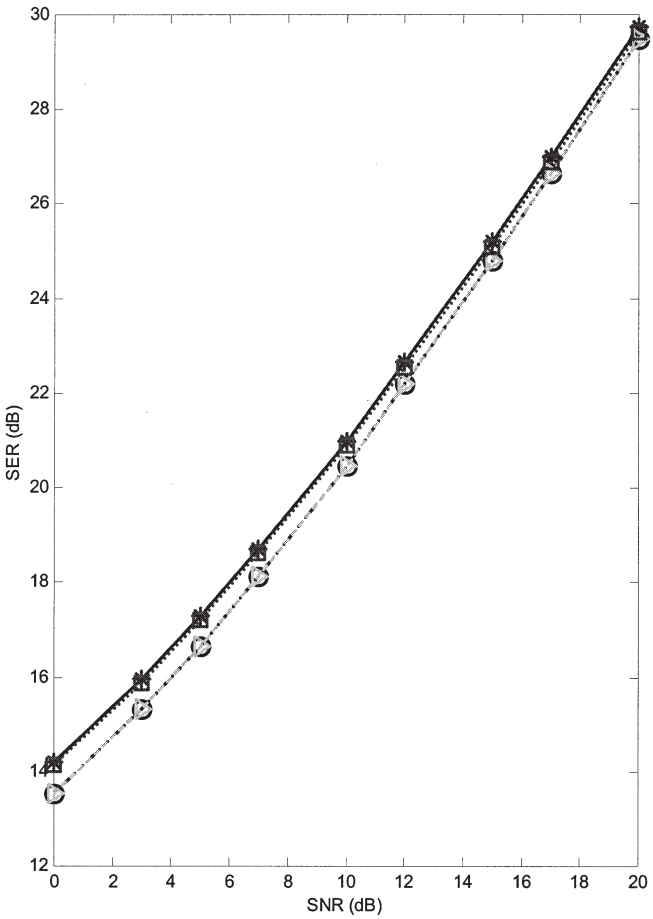

Figure 3. Performance of the four algorithms, SVD (circle), ML (square), LS (star), and SoS (triangle), shown in terms of image reconstruction SER (dB) vs. measurement SNR (dB). Clearly, ML and LS perform almost identically outperforming SVD and SoS, which also perform identically.

synthetic data are presented in Fig. 3 in terms of average reconstruction SER vs. measurement SNR for all algorithms. These experiments show that all four algorithms asymptotically (as the SNR approaches infinity) achieve equivalent reconstruction SER levels. For low SNR, however, although SVD and SoS yield the same level of SER performance, the ML and LS algorithms provide a slight (about 0.6 dB) gain in SER.

As a second case study, all four algorithms are applied to the multiple coil images presented in Fig. 1a–d, which are collected by the coil array shown in Fig. 1e (with the previously specified measurement parameters). For the two iterative methods (ML and LS), the SoS estimate of the coil sensitivity profiles and image intensities are utilized as initial conditions. In addition, for both SVD and ML algorithms, 5×5 non-overlapping regions in which the coil sensitivity is assumed to be constant are used, and the scale ambiguity for the solution of each region is resolved by normalizing the power of the reconstructed signal for that region to that of the SoS reconstruction. The ML algorithm uses a noise covariance estimate $\mathbf{\Psi}$ obtained from a purely noise region of the coil images, and in an ad-hoc manner, the covariance of the coil sensitivity distribution is assumed to be $\Lambda = \mathbf{I}$. Also quite heuristically, in the LS algorithm, all three weight parameters are set to $\lambda_i = 0.1$.[5] In phased array MRI, the quality of reconstructed images is often quantified by SNR, as the "true" image is usually unknown.[6] The reconstructed images obtained by these four methods, as well as the estimated local SNR levels of these reconstructed images are presented in Fig. 4. By comparing the SNR estimates in Fig. 4e–h, we observe that the SVD and SoS methods, in general, produce images with equal SNR levels (although SVD is observed to be more sensitive to noise and measurement artifacts as discussed below), whereas the ML approach improves the SNR by up to 2 dB and the LS approach improves the SNR by up to 3 dB over the performance of SoS.

At first look, a clear artifact in the SVD reconstructed image shown in Fig. 4a is visible. Although this artifact is not as visible in the other three reconstructed images (Fig. 4b–d) due to the small size of the figures, on closer look, we see that this horizontal artifact also exist in these images. The reason for this artifact is identified as a horizontal measurement artifact that exists in all four coil measurements at that location (most strongly seen in the first coil). This artifact, along with measurement noise, is amplified in the SVD reconstruction method to the highly visible level in Fig. 4a. The reason for this amplification of noise and outliers can be understood by investigating Fig. 2b. The ratios of the maximum singular values to minimum ones are not as large in the top half of the coil measurement image as the same ratios in the bottom half of the image. Consequently, A3 is not as strongly satisfied in the top half as the bottom half. This causes the SVD algorithm to pass the existing measurement noise to the reconstructed image with some amplification. The artifact in the measurements is also amplified in the process.

DISCUSSION

Phased-array MRI research has experienced an increased interest in the last decade due to the potential gains in both imaging quality and acquisition speed. Although many algorithms have been proposed for phased-array MR image reconstruction, in addition to the perhaps most commonly used sum-of-squares al-

[5]Experiments performed to establish an understanding of how these parameters affect the reconstruction performance demonstrated that extreme values (both in smaller and larger directions) degrade the quality of the image. In general, the authors observed that for all three coefficients values in the interval (0.05,0.1) are reasonable. Values greater than 0.1 tend to overemphasize the penalty functions, while values smaller than 0.05 do not provide sufficient smoothing.

[6]The SNR calculated here (given in dB scale) is the ratio of the power of the reconstructed image intensity in the region of interest to the power of the reconstructed image intensity in a reference region, which presumably consists only of noise. Under the spatially WSS noise assumption, the SNR calculated using this method is on average equal to the SNR+1 (in linear scale), where the latter is the conventional definition common in the signal processing literature. In the examples shown in Fig. 4, a rectangular region at the top left corner, which consists of pure noise, is selected as the reference noise power region. The SNR in the other rectangular regions, as shown in Fig. 4, are calculated by dividing the signal power in the selected region by the noise power estimated from the reference region. The values are then converted to decibels using the $10\log_{10}(.)$ formula.

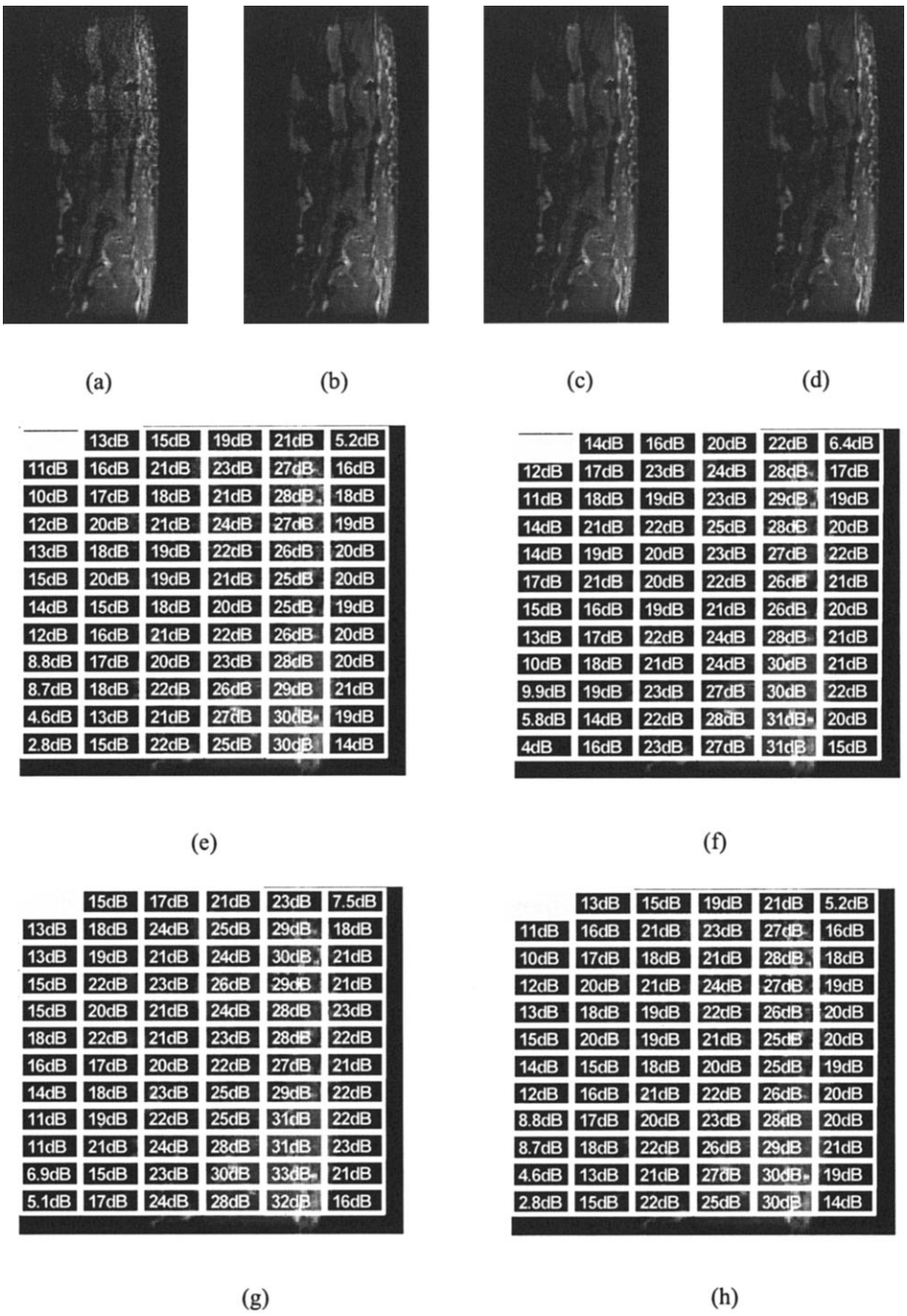

Figure 4. The reconstructed images using SVD (**a**), ML (**b**), LS (**c**), and SoS (**d**) approaches and their estimated local SNR levels SVD (**e**), ML (**f**), LS (**g**), and SoS (**h**), where the top left region is the noise reference. Notice that in e–h, the SNR levels are overlaid on the reconstructed image of the corresponding method. To prevent the numbers from squeezing, these images are stretched horizontally. The top left corner of each image is used as the noise power reference.

gorithm, these approaches are not based on a statistical or optimal signal processing framework.

In this paper, the problem of combining images obtained from multiple MRI coils is studied from a statistical signal processing point of view with the goal of improving SNR in the reconstructed images. In order to pursue this approach, certain model assumptions must be made. We developed a set of assumptions that were observed to hold on data collected from real measurements, and three alternative algorithms, stemming from well-established statistical signal processing techniques, and founded on these assumptions were proposed.

Our new proposed methods, namely singular value decomposition, maximum-likelihood, and least-squares with smoothness penalty, were evaluated on synthetic and real data collected from a four-coil phased array using a 4.7-T scanner for small animals. A quantitative analysis of the reconstructed images obtained using measurements of a cat spinal cord revealed that it is possible to improve the quality of the final images (in terms of local SNR) by up to 2 dB using the maximum-likelihood approach and up to 3 dB using the LS approach.

There are still unsolved issues, however. For example, if the original measurements already have high SNR, then the reconstructed image using SoS performs

close to maximum ratio combining (25); therefore a few dB of gain in reconstruction SNR may not be visible to the human eye. With the maximum-likelihood approach, we used the standard circular-Gaussian noise model; yet, we ended up with a relatively complicated expression that needs to be maximized. More accurate statistical signal models might improve the performance of our approach; nevertheless, computational complexity is always a concern for MRI.

The SNR is a convenient and widely used quality assessment instrument for MR images. The use of the singular value decomposition and least-squares methods statistically make sense when this second order quantity is utilized for quality assessment. On the other hand, other quantitative measures such as signal-to-contrast ratio might be more representative of image quality as perceived by a human observer. In that case, alternative optimization criteria for optimal reconstruction of the coil measurements must be derived. These alternative criteria must be consistent with the desired quality measure, as well as being sufficiently simple for low-complexity optimization procedures to be practical.

ACKNOWLEDGMENTS

The authors thank Barbara Beck, Jim Caserta, and Dave Peterson for collecting the cat spine measurements at the McKnight Brain Institute of the University of Florida, as well as their valuable comments during many discussions.

APPENDIX A

Maximizing the expression in Eq. [9] is difficult, or at least computationally burdensome. Although it is possible to determine a closed-form expression for the gradient with respect to ρ, we have used the argument of the integral as an approximation to the whole expression:

$$F(\mathbf{c},\rho) = \|(\mathbf{S} - \rho\mathbf{c}^T)\mathbf{\mathfrak{Q}}^{-1/2}\|^2 + \|\Lambda^{-1/2}(\mathbf{c} - \mu)\|^2 \quad (A.1)$$

To maximize the term in Eq. [A1], we propose the following cyclic optimization algorithm, which minimizes the criterion by alternately updating ρ and $\mathbf{c}$:

1. Initialize μ to $\mathbf{0}$, and ρ to ρ_0. Select T and set $i = 0$. Alternatively, μ could be set to the SoS estimate of $\mathbf{c}$. Also, ρ_0 can be set to the SoS reconstruction result.
2. Compute $\mathbf{c}_0 = \arg\min_c F(\mathbf{c},\rho_0)$.
3. Let $\mu = \mathbf{c}_i$. Compute $\rho_{i+1} = \arg\min_\rho F(\mathbf{c}_i,\rho)$ and $\mathbf{c}_{i+1} = \arg\min_c F(\mathbf{c},\rho_{i+1})$
4. If $F(\mathbf{c}_{i+1},\rho_{i+1}) - F(\mathbf{c}_i,\rho_i) < T$ go to 6.
5. Increment i and go to 3.
6. Assign $\hat{\rho} = \rho_{i+1}$ and $\hat{\mathbf{c}} = \mathbf{c}_{i+1}$.

Because Eq. [A1] is a quadratic function in both ρ and $\mathbf{c}$, we easily find that:

$$\begin{aligned}\mathbf{c}_{i+1} &= [\mathbf{T}_j^H\mathbf{T}_i + \Lambda^{-H/2}\Lambda^{-1/2}]^{-1}[\mathbf{T}_i^H\tilde{\mathbf{S}} + \Lambda^{-H/2}\tilde{\mu}] \\ \rho_{i+1} &= [\mathbf{B}_i^H\mathbf{B}_i]^{-1}\mathbf{B}_i^H\tilde{\mathbf{S}}\end{aligned} \quad (A.2)$$

where $\mathbf{T}_i = \mathbf{\mathfrak{Q}}^{-T/2} \otimes_{\rho i}$, $\mathbf{B}_i = (\mathbf{\mathfrak{Q}}^{-T/2}\mathbf{c}_i) \otimes \mathbf{I}$, $\tilde{\mu} = \Lambda^{-1/2}\mu$, $\mathbf{T}_i = \mathbf{\mathfrak{Q}}^{-T/2} \otimes_{\rho i}$, $\mathbf{B}_i = (\mathbf{\mathfrak{Q}}^{-T/2}\mathbf{c}_i) \otimes \mathbf{I}$, $\tilde{\mu}=\Lambda^{-1/2}\mu$, and $\tilde{\mathbf{S}} = (\mathbf{\mathfrak{Q}}^{-T/2} \otimes \mathbf{I})[\mathbf{s}_1^T \ldots \mathbf{s}_{n_c}^T]^T$ are defined using the Kronecker product $\otimes$.

APPENDIX B

The criterion in Eq. [10] can be minimized using standard optimization techniques (37). However, the function may have several local minima that can render the reconstruction sub-optimal. One possible optimization algorithm is the conjugate gradient (CG) method. The gradient $\mathbf{G}$ of the cost function in Eq. [10] with respect to the optimization variables $\mathbf{W} = [\rho^T,\mathbf{c}_1^T,\ldots,\mathbf{c}_{n_c}^T]^T$ is given in Eq. [B1] where $\circ$ denotes element-wise vector product. In Eq. [B1], $\mathbf{A}_i$ and $\mathbf{B}_i$ are non-symmetric sparse Toeplitz matrices that arise from the matrix formulation of the first and second order differences. In particular, $\mathbf{A}_1$ and $\mathbf{A}_2$ are $(M_1-1) \times M_1$ and $(M_2-1) \times M_2$ matrices with 1s on the main diagonal and –1s in the first upper diagonal, and $\mathbf{B}_1$ and $\mathbf{B}_2$ are $(M_1-2) \times M_1$ and $(M_2-2) \times M_2$ matrices with 1s on the main diagonal, –2s in the first upper diagonal, and 1s in the second upper diagonal. All other entries of these matrices are zeros. Similar to the case of the Bayesian reconstruction algorithm, obtaining an asymptotic SNR expression for this algorithm should be possible although it is algebraically complicated:

$$\begin{aligned}\mathbf{G} &= \begin{bmatrix} \partial J/\partial\rho \\ \partial J/\partial\mathbf{c}_1 \\ \vdots \\ \partial J/\partial\mathbf{c}_{n_c} \end{bmatrix} = (1 - \lambda_1 - \lambda_2 - \lambda_3)\mathbf{G}_0 \\ &\quad + \lambda_1\mathbf{G}_1 + \lambda_2\mathbf{G}_2 + \lambda_3\mathbf{G}_3 \\ \mathbf{G}_0 &= \begin{bmatrix} \partial J_0/\partial\rho \\ \partial J_0/\partial\mathbf{c}_1 \\ \vdots \\ \partial J_0/\partial\mathbf{c}_{n_c} \end{bmatrix} = \begin{bmatrix} 2\sum_{k=1}^{n_c}[\rho \circ \mathbf{c}_k \circ \mathbf{c}_k - \mathbf{s}_k \circ \mathbf{c}_k] \\ [\mathbf{c}_1 \circ \rho \circ \rho - \mathbf{s}_1 \circ \rho] \\ \vdots \\ [\mathbf{c}_{n_c} \circ \rho \circ \rho - \mathbf{s}_{n_c} \circ \rho] \end{bmatrix} \\ \mathbf{G}_1 &= \begin{bmatrix} \partial J_1/\partial\rho \\ \partial J_1/\partial\mathbf{c}_1 \\ \vdots \\ \partial J_1/\partial\mathbf{c}_{n_c} \end{bmatrix} = \begin{bmatrix} \mathbf{0} \\ 2(\mathbf{A}_1^T\mathbf{A}_1\mathbf{c}_1 + \mathbf{c}_1\mathbf{A}_2^T\mathbf{A}_2) \\ \vdots \\ 2(\mathbf{A}_1^T\mathbf{A}_1\mathbf{c}_{n_c} + \mathbf{c}_{n_c}\mathbf{A}_2^T\mathbf{A}_2) \end{bmatrix} \\ \mathbf{G}_2 &= \begin{bmatrix} \partial J_2/\partial\rho \\ \partial J_2/\partial\mathbf{c}_1 \\ \vdots \\ \partial J_2/\partial\mathbf{c}_{n_c} \end{bmatrix} = \begin{bmatrix} \mathbf{0} \\ 2(\mathbf{B}_1^T\mathbf{B}_1\mathbf{c}_1 + \mathbf{c}_1\mathbf{B}_2^T\mathbf{B}_2) \\ \vdots \\ 2(\mathbf{B}_1^T\mathbf{B}_1\mathbf{c}_{n_c} + \mathbf{c}_{n_c}\mathbf{B}_2^T\mathbf{B}_2) \end{bmatrix} \\ \mathbf{G}_3 &= \begin{bmatrix} \partial J_3/\partial\rho \\ \partial J_3/\partial\mathbf{c}_1 \\ \vdots \\ \partial J_3/\partial\mathbf{c}_{n_c} \end{bmatrix} = \begin{bmatrix} 2\rho \\ \mathbf{0} \\ \vdots \\ \mathbf{0} \end{bmatrix}\end{aligned} \quad (B.1)$$

REFERENCES

1. McVeigh E, Ozturk C. Imaging myocardial strain. IEEE Signal Processing Magazine 2001;18:44–56.

2. Roemer PB, Edelstein WA, Hayes CE, Souza SP, Mueller OM. The NMR phased array. Magn Reson Med 1990;16:192–225.
3. Hutchinson M, Raff U. Fast MRI data acquisition using multiple detectors. Magn Reson Med 1988;6:87–91.
4. Hayes CE, Hattes N, Roemer PB. Volume imaging with MR phased arrays. Magn Reson Med 1991;18:309–319.
5. Kwiat D, Einav S, Navon G. A decoupled coil detector array for fast image acquisition in magnetic resonance imaging. Med Phys 1991; 18:251–265.
6. Wright SW, Porter JR. Parallel acquisition of MR images using time multiplexed coils. Electronics Letters 1992;28:71–72.
7. Ra JB, Rim CY. Fast imaging using sub-encoding data sets from multiple detectors. Magn Reson Med 1993;30:142–145.
8. Carlson JW, Minemura T. Imaging time reduction through multiple receiver coil data acquisition and image reconstruction. Magn Reson Med 1993;29:681–688.
9. Wright SM, Wald LL. Theory and application of array coils in MR spectroscopy. NMR Biomed 1997;10:394–410.
10. Pruessmann KP, Weiger M, Scheidegger MB, Boesiger P. SENSE: sensitivity encoding for fast MRI. Magn Reson Med 1999;42:952–962.
11. Weiger M, Pruessmann KP, Boesiger P. 2D SENSE for faster 3D MRI. MAGMA 2002;14:10–19.
12. Sodickson DK, Manning WJ. Simultaneous acquisition of spatial harmonics (SMASH): fast imaging with radiofrequency coil arrays. Magn Reson Med 1997;38:591–603.
13. Sodickson DK, Griswold MA, Jakob PM, Edelman RR, Manning WJ. Signal-to-noise ratio and signal-to-noise efficiency in SMASH imaging. Magn Reson Med 1999;41:1009–1022.
14. Jakob PM, Griswold MA, Edelman RR, Sodickson DK. AUTO-SMASH: a self-calibrating technique for SMASH imaging. MAGMA 1998;7:42–54.
15. Sodickson DK, McKenzie CA, Ohliger MA, Yeh EN, Price MD. Recent advances in image reconstruction, coil sensitivity calibration, and coil array design for SMASH and generalized parallel MRI. MAGMA 2002;13:158–163.
16. Griswold MA, Jakob PM, Nittka M, Goldfarb JW, Haase A. Partially parallel imaging with localized sensitivities (PILS). Magn Reson Med 2000;44:602–609.
17. Bloch F. Nuclear induction. Phys Rev 1946;70:460–473.
18. Haacke EM, Brown RW, Thompson MR, Venkatesan R. Magnetic resonance imaging—physical principles and sequence design. New York: John Wiley and Sons; 1999. 914 p.
19. Wright GA. Magnetic resonance imaging. IEEE Signal Processing Magazine 1997;14:56–66.
20. De Beer R, Marseille GJ, Mehikopf AF, Van Ormondt D, Wajer FTAW. Modeling of medical magnetic resonance imaging signals. IEEE Proc Vision Image Signal Processing 1994;141:71–75.
21. Edelstein WA, Glover GH, Hardy CJ, Redington RW. The intrinsic signal-to-noise ratio in NMR imaging. Magn Reson Med 1986;3: 604–618.
22. Hayes CE, Roemer PB. Noise correlations in data simultaneously acquired from multiple surface coil arrays. Magn Reson Med 1990; 16:181–191.
23. Duensing GR, Brooker HR, Fitzsimmons JR. Maximizing signal-to-noise ratio in the presence of coil coupling. J Magn Reson 1996; 111:230–235.
24. Horn RA, Johnson CR. Matrix analysis. Cambridge: Cambridge University Press; 1985.
25. Larsson EG, Erdogmus D, Yan R, Principe JC, Fitzsimmons JR. SNR-optimality of sum-of-squares reconstruction for phased-array magnetic resonance imaging. J Magn Reson 2003;163:121–123.
26. Debbins JP, Felmlee JP, Riederer SJ. Phase alignment of multiple surface coil data for reduced bandwidth and reconstruction requirements. Magn Reson Med 1997;38:1003–1011.
27. Bydder M, Larkman DJ, Hajnal JV. Combination of signals from array coils using image-based estimation of coil sensitivity profiles. Magn Reson Med 2002;47:539–548.
28. Kellman P, McVeigh ER. Ghost artifact cancellation using phased array processing. Magn Reson Med 2001;46:335–343.
29. Walsh DO, Gmitro AF, Marcellin MW. Adaptive reconstruction of phased array MR imagery. Magn Reson Med 2000;43:682–690.
30. Murakami JW, Hayes CE, Weinberger E. Intensity correction of phased array surface coil images. Magn Reson Med 1996;35:585–590.
31. Papoulis A. Probability, random variables, and stochastic processes. New York: McGraw-Hill; 1991. p 214.
32. Yee KS. Numerical solution of initial boundary value problems involving Maxwell's equations in isotropic media. IEEE Trans Antennas Propagation 1996;14:302–307.
33. Kunz KS, Luebbers RJ. The finite difference time domain method for electromagnetics. Boca Raton: CRC Press; 1993. 448 p.
34. Ibrahim TS, Lee R, Baertlein BA, Kangarlu A, Robitaille PML. Application of finite-difference time-domain method for the design of birdcage RF head coils using multi-port excitations. Magn Reson Med 2000;18:733–742.
35. Kitagawa G, Gersch W. A smoothness priors time-varying (AR) coefficient modeling of nonstationary covariance time series. IEEE Trans Automatic Control 1985;30:48–56.
36. Kay SM. Fundamentals of statistical signal processing: estimation theory. Englewood Cliffs: Prentice Hall; 1993. p 162–164.
37. Luenberger DG. Linear and nonlinear programming. Boston: Addison-Wesley; 1973. 491 p.